EUROPEAN FUSION DEVELOPMENT AGREEMENT

EFDA–JET–PR (01)44

V. Tribaldos

Spatial Resolution of the Electron Cyclotron Emission at JET

Spatial Resolution of the Electron Cyclotron Emission at JET

[1]V. Tribaldos and contributors to the EFDA-JET workprogramme*

[1]Laboratorio Nacional de Fusion
Asociación EURATOM-CIEMAT para la Fusión
Avenida Complutense 22, 28040 Madrid, Spain

** See annex of J. Pamela et al. "Overview of Recent JET Results and Perspectives", Fusion Energy 2000 (Proc. 18th Int. Conf. Sorrento, 2000), IAEA, Vienna (2001).*

ABSTRACT

The purpose of this report is to obtain estimations of the spatial resolution of the Electron Cyclotron Emission (ECE) phenomena for the typical plasmas found in JET tokamak. The analysis of the spatial resolution of the ECE is based on the underlying physical process of emission and a working definition is presented and discussed. In making these estimations a typical JET pulse is being analysed taking into account the magnetic configuration, the density and temperature profiles, obtained with the EFIT code and from the LIDAR diagnostic. Ray tracing simulations are performed for a Maxwellian plasma taking into account the antenna pattern.

Pacs: 52.55Fa, 52.25Sw, 52.70Gw, 52.65

1. INTRODUCTION

The Electron Cyclotron Emission (ECE) is a convolution of the emission and absorption processes taking place in a magnetically confined plasma near the electron cyclotron frequency and its harmonics. Its theory is well known [1] and its capabilities for measuring the electron temperature are used routinely in almost every fusion device. The information contained in the ECE signal is a complicate function of several factors along the line of sight, namely: the gradient of the magnetic field modulus, the angle between the viewing direction and the magnetic field, and local the density and temperature.

The intensity of the EC emission received, for a given frequency, is equal to the integral of the intensity emitted by the participating particles, at that frequency, reduced by the fraction that is actually transmitted as it travels towards the detection system.

$$I(\omega) = \beta(l)\exp\left[-\int \alpha(l')\,l\,dl'\right] dl \qquad (1)$$

In the literature this expression is known as the solution of the radiative transfer equation [2], which is an equation for the conservation of the radiating energy. In general eq. (1) not only applies to the ECE emission but to a broader class of plasma emission processes each with its own expressions for the emission, β, and absorption, α, coefficients, i.e.; soft and hard X-ray emission, spectroscopic emissions, bolometry; although, for these processes the absorption plays a negligible role.

When the distribution function of the electrons in the plasma is Maxwellian the emitted intensity is related to the electron temperature. This is because for thermal plasmas the emission and absorption coefficients are proportional, and is usually referred as the Kirchhoff´s law of radiation

$$\beta(\mathrm{r}) = \left(\frac{\omega}{c}\right)^2 \frac{T_e(\mathrm{r})}{(2\pi)^3}\ \alpha(\mathrm{r}) \qquad (2)$$

** See annex of J. Pamela et al. "Overview of Recent JET Results and Perspectives", Fusion Energy 2000 (Proc. 18th Int. Conf. Sorrento, 2000), IAEA, Vienna (2001).*

Inserting in eq. (1) the expression of β of eq. (2)

$$I(\omega) = \frac{1}{(2\pi)^3} \left(\frac{\omega}{c}\right)^2 \int T_e(l)\alpha(l)\exp\left[\int_{-\infty}^{l} \alpha(l')\, dl'\right] dl \qquad (3)$$

we found that the intensity is a convolution between the electron temperature profile and the self-absorption. If we now define the transmission coefficient

$$T(l) = \exp\left[\int_{-\infty}^{l} \alpha(l')\, dl'\right] \equiv \exp[-\tau(l)] \qquad (4)$$

eq. (4) can be written, normalising the emitted intensity in units of temperature, as

$$T_{ECE}(\omega) = -\int T_e(l) \frac{dT(l')}{dl'} dl \qquad (5)$$

For plasma conditions where a certain harmonic (and propagation mode) of the electron cyclotron resonance is highly absorbed (the total transmission T is very low, or the optical depth, τ, is very high) the variation of the transmission coefficient, T, display a peaked shape *around*[§] the resonance region, see Fig.1. If the typical variation length of the temperature profile is larger than the width of the transmission profile it is possible to approximate the integral of eq. (5) as

$$T_{ECE}(\omega) \approx -T_e(\bar{l}) \int \frac{dT(l')}{dl'} dl = T_e(\bar{l})\{1-T\} \qquad (6)$$

$$= T_e(\bar{l})\{1-exp[-\tau]\} \approx T_e(\bar{l})$$

and the emitted intensity is a measure of the local electron temperature in that region. This is precisely the reason why the EC emission a valuable tool in fusion devices, because it is a local measurement of the electron temperature

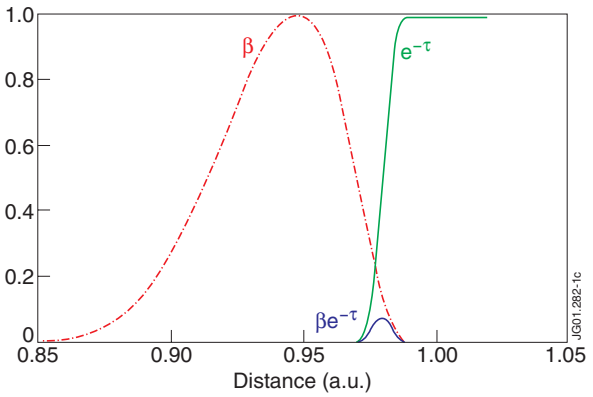

Figure 1: Sketch of emission, β, transmission, T, and emitting profiles.

[§] *The actual region where the transmission profile has its peak depends on the frequency and on the angle between the viewing direction and the magnetic field ($N_{||}$)*

However, it is important to notice the approximations we have made in arriving to this conclusion:

1. The electron distribution function is assumed to be Maxwellian. In facing with non-thermal electron distribution functions Kirchhoff´s radiation law does not hold, the emission and absorption coefficients are not proportional, and although the rest of the conditions may be fulfilled, the measured intensity is not necessarily related to the electron temperature. Temperature is a quantity that it is only defined rigorously for Maxwellian distribution functions, i.e.; it is a measure of how fast the number of particles decrease with energy.

2. The absorption of electromagnetic waves near the electron cyclotron frequency or some of its harmonics is assumed to be very high, at least for one of the two propagating modes. The EC absorption coefficient, α, is a complicated function depending on the harmonic (1st, 2nd,…), the mode of propagation (Ordinary or eXtraordinary), the plasma parameters (density and temperature) and the angle between the magnetic field, **B**, and the wave vector **k**. ($N_{\|}$). It is well known that the best absorbed harmonics and modes are the first harmonic O-mode and the second harmonic X-mode (although for some plasma conditions the second harmonic O-mode and the third harmonic X-mode are also very well absorbed, see next sections). For these modes the absorption coefficient increases linearly with the density and more than linearly with the temperature, thus the plasma should be dense and hot enough. However, these conditions are not necessarily fulfilled in certain plasma regions, i.e.; the plasma edge. Finally, since the absorption coefficient decreases as $N_{\|}$ increases a favourable viewing direction with a narrow antenna pattern is necessary. It is also possible that in some devices for some frequencies the emission from different harmonics overlap thus destroying the locality.

3. The typical variation length of the temperature profile is assumed to be larger than the width of the derivative of the transmission co-efficient. Therefore, if the electron temperature profile is known to vary strongly inside the emitting region the measured intensity can only be regarded as an average of the electron temperature. It acts as a high-pass filter.

From the above points it should be clear that there are some limitations in using the EC emission as a diagnostic tool for measuring the local electron temperature. For a given fusion device some of the problems can be address by choosing the best viewing direction, the right harmonic and propagation mode. Unfortunately, there are other limitations depending on the plasma parameters (low density and/or temperature, non Maxwellian electron distribution functions due to auxiliary heating,…) or the device itself (harmonics overlapping due to the magnetic field gradient, lack of space for placing the antennas in the best positions, large magnetic field shear,…). In this later case it is then necessary to establish the operational bounds of the diagnostic set-up in order to make the correct interpretation of the measurements.

The aim of the present report is to discuss the spatial resolution of the EC emission diagnostic of JET tokamak in measuring the electron temperature profile. The report is organised as follows:

in Section 2 a very brief description of JET tokamak is given in regards to the relevant EC physics, along with the actual diagnostic systems in use; the details of the method for calculating the spatial resolution is presented in Section 3; the results obtained for a test case are presented in Section 4; finally some conclusions are drawn in Section 4.

2. ECE AND JET TOKAMAK

JET is a large, iron core, tokamak of non-circular cross section (D-shape), equipped with a divertor, whose main parameters are described in Table 1. Its magnetic field is mainly produced by a set of 32, equally spaced, toroidal field coils.

Parameter		
Plasma major radius		2.96 m
	Horizontal	1.25 m
Plasma minor radius		
	Vertical	2.10 m
Pulse length		20 s
Magnetic field on axis		3.45 T
Plasma Current		4.8 MA
Additional Heating Power		25 MW

Table 1: Main JET parameters

There are two operational ECE systems now at JET, known as KK1 and KK3. KK1 is a Michelson interferometer viewing the plasma column along the equatorial plane of the plasma from the low field side. KK3 is a 48 channel heterodyne radiometer also viewing the plasma in the same direction as KK1 but 15 cm bellow the equatorial plane of the plasma. The components facing the plasma are two rectangular *open waveguides* of dimensions 6 • 5 cm, that to a first approximation gives an antennae pattern similar to a rectangular grid Fraunhoffer diffraction pattern, see Fig.2.

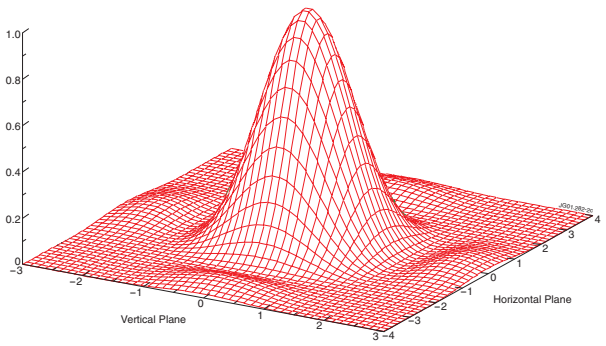

Figure 2: Antenna pattern corresponding to the actual open waveguides of KK1 and KK3 systems simulated as the Fraunhoffer diffraction pattern of a rectangular grid.

Whereas the Michelson interferometer system distance between channels is limited by the maximum speed at which the linear mirror moves, in the KK3 radiometer an especial effort have been made in optimising the filters´ bandwidth (250 MHz with almost square shape) and the distance between consecutive channels (500 MHz). Later on, when discussing the spatial resolution of the system, the contribution due to these parameters will be compared to other broadening mechanisms.

As will be seen in next section, for computing the spatial resolution a detailed description of the device and the plasma parameters are necessary. Since a ray tracing procedure will be used, the magnetic field, the density and the electron temperature are needed as a function of the position. The easiest way to accomplish with these requirements is to express the magnetic field and the experimental density and temperature profiles as a function of the magnetic surfaces and defines a transformation of coordinates between real space and magnetic surfaces. To obtain the coordinate transformation the plasma magnetic flux (magnetic surfaces), solution of the equilibrium code EFIT [3], is stored on a grid in real space. Then the electron density and temperature profiles, obtained from the LIDAR Thomson scattering system [4], are transformed from major radius, R, to magnetic surfaces by making a two-dimensional spline interpolation on the grid. Finally the profiles dependencies on the magnetic flux are fitted to obtain the local density and temperature at any point in the plasma. In making these transformations a small asymmetry was notice in the density and temperature profiles, see Fig.3. This asymmetry was clearer in the temperature profile. Since the pressure should be constant on the magnetic surfaces it seems that there is a disagreement between the EFIT and LIDAR data. This discrepancy is shown in Fig.3 were the profiles are

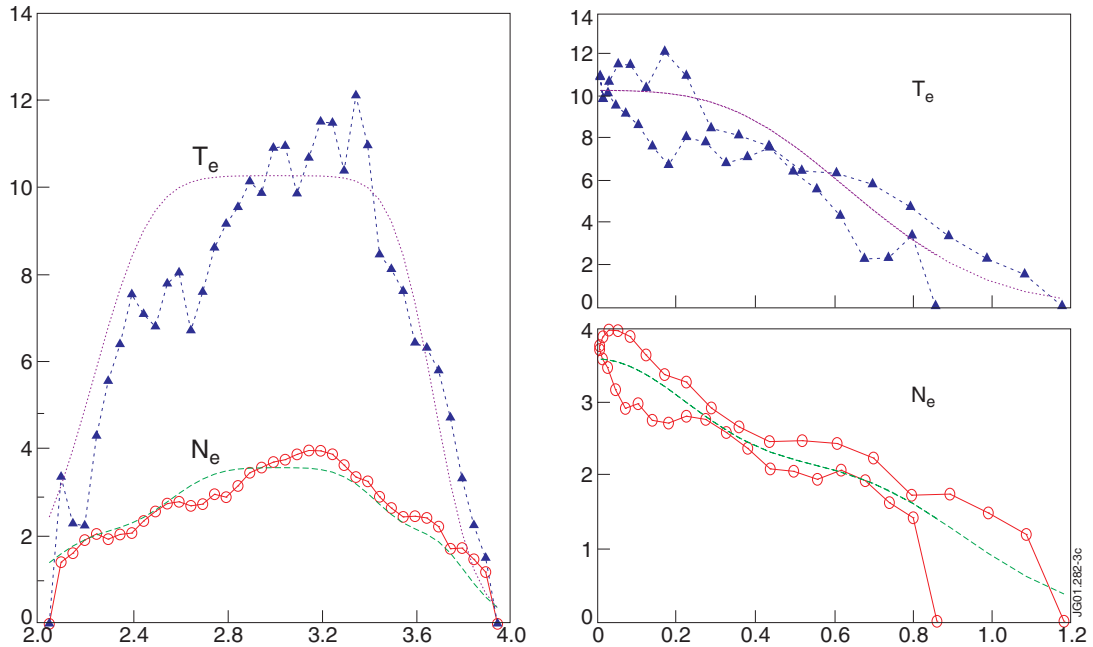

Figure 3: On the right density (10^{19} m^{-3}) and electron temperature (keV) profiles, obtained with the LIDAR Thomson scattering for the shot #47413. On the left the same profiles versus the normalised magnetic flux obtained with the EFIT equilibrium code

unfolded in magnetic surfaces. The reason for the disagreement is under investigation, however, from the operational point of view a possible way to deal with the difference, and continue with the calculations, consist in shifting the whole LIDAR profiles in major radius by approximately 10 cm inward. In Fig.4 the same profiles shifted 10 cm are presented as in Fig.3.

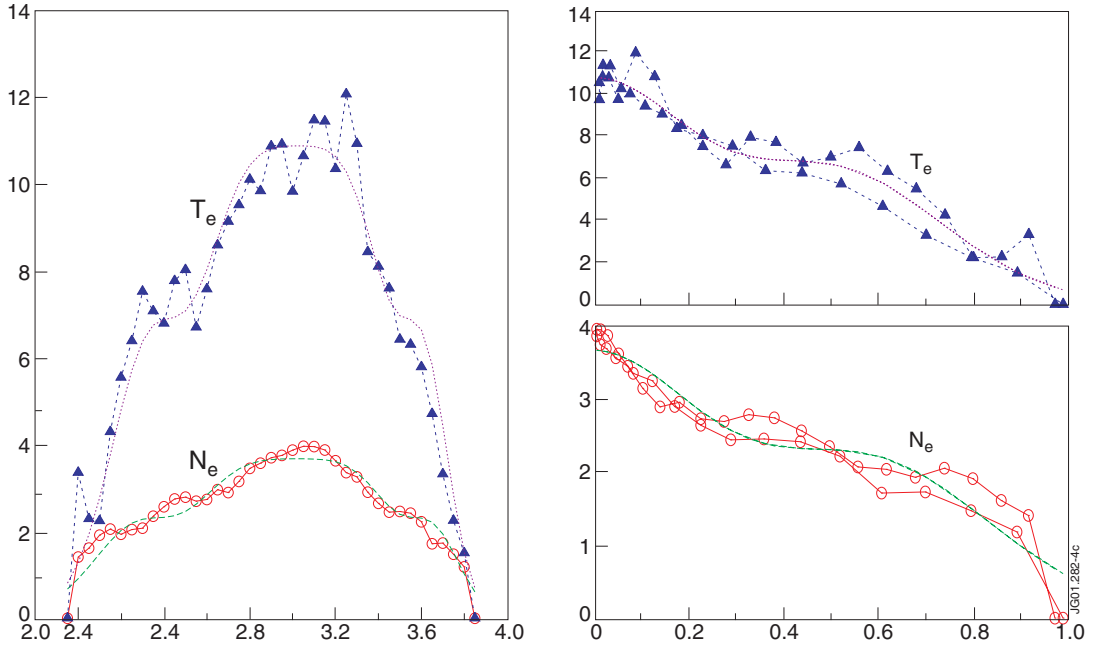

Figure.4: The same as in Fig. 3 but with the profiles shifted by 10 cm in major radius.

The above density, temperature and magnetic field, defined at any point inside the plasma, was introduced in the TRECE 3-D ray tracing code to simulate the electron cyclotron emission spectra for the real viewing conditions of the ECE experimental set-up of KK1. In Fig.5 the trajectories of the rays, for KK1 and KK3. The spectra obtained from the KK1 Michelson interferometer is plotted in Fig.6 with the simulations of the ray tracing code. The agreement between the measured spectra and the simulated one make us confident that the description of the plasma is good enough to proceed with the rest of the simulations. The spectra also display the problem of harmonic overlapping, which is very clear in between the 2nd and 3rd harmonics of the X-mode. Moreover, the signal received

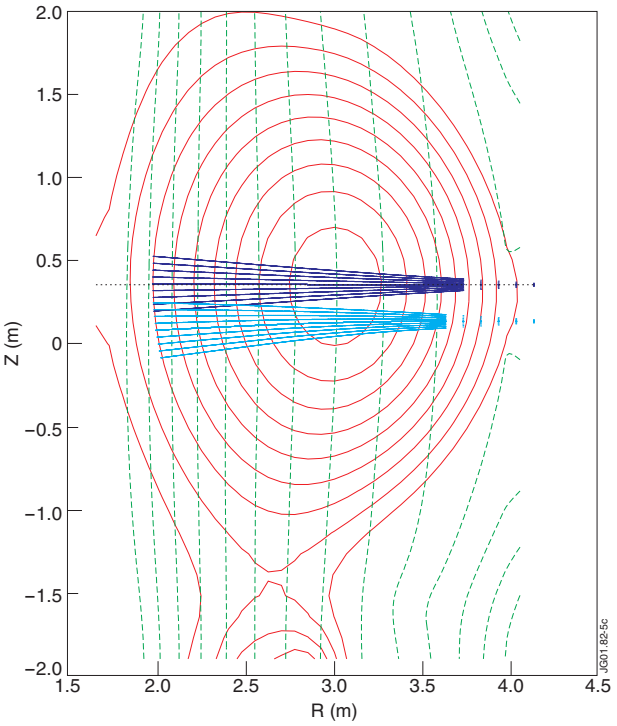

Figure.5: Ray tracing simulation of the KK1, in blue, and KK3, in red, systems now in operation at JET for the conditions of shot #47413.

at low frequency seems to indicate that a certain fraction of O-mode emission is being detected in the Michelson, although it is supposed to measure only the Xmode emission.

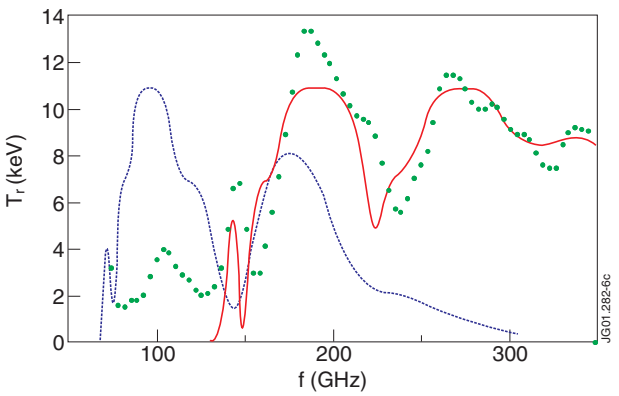

Figure.6: Electron cyclotron emission spectra, in temperature units, for the shot #47413 obtained with the KK1 Michelson interferometer and simulated with the ray tracing the first harmonic O-mode and second harmonic X-mode.

3. PROCEDURE DESCRIPTION

The favourable conditions for measuring the electron temperature by means of the EC emission are those with high absorption. The dependence of the absorption coefficient on the plasma parameters (density and temperature), the harmonic of the cyclotron frequency, the propagation mode, and the angle between the observation direction and the magnetic field, $N_{||} = \mathbf{k} \bullet \mathbf{B}/|\mathbf{k}|\,|\mathbf{B}|$, is well known. Most of the ECE detection systems installed in fusion devices are observing the emission in the 1st harmonic O-mode or the 2nd harmonic X-mode, in a direction perpendicular to the magnetic field ($N_{||} = 0$). For a given observation frequency, f, and perpendicular observation, $N_{||} = 0$, using the resonant condition, $\gamma - s f_c / f - N_{||} u_{||} = 0$ (where γ is the usual relativistic factor, s is the harmonic, $fc = e|\mathbf{B}(\mathbf{r})|/mc$ is the cyclotron frequency, f the observation frequency, and $\mathbf{u} = \mathbf{p}/mc$) it is possible to relate the energy of the resonant electrons to the local magnetic field, along the line of sight: $E = mc^2(\gamma - 1) = mc^2\,(s f_c - f)/f$. The energy of the resonant electrons increases with the difference between the local resonance and the observation frequency ($s f_c > f$), and only zero energy electrons can resonate at $f = s f_c$. Unfortunately, it is usual to associate the origin of the emission, at a certain frequency, f, precisely with that position, although no emission is generated there.

The emission of the plasma in the electron cyclotron frequency range, even for the best conditions, i.e.: for thermal electron distribution functions (Maxwellian), the best absorbing harmonics and modes, and the optimum viewing conditions, is originated in a finite plasma region. In this section we are to present a general method for estimating the plasma volume contributing to the EC emission, that in the next section will be applied to the particular case of the two systems in operation at JET.

The easiest way to proceed is just to start with the solution of the radiative transfer equation, Eq. 1, and plot the different terms entering in the emission calculations, namely: the local emission, β, absorption, α, and transmission, T, coefficients. In Fig.7 these terms are plotted versus the major radius for a line on sight in the equatorial plane of the plasma for the second harmonic X-mode at $f = 195$ GHz. In computing the transmission coefficient it is assumed that the emission is detected from the low field side. To study the dependence of the emission on the temperature and the density three plasma conditions are presented, all with the shape of the profiles corresponding to the shot #47413 but with different central values (see Table 2).

Case	Te(0) [keV]	N(0) [10^{19} m^{-3}]
1(#47413)	10.9	3.7
2	2	3.7
3	10.9	7

Table 2: Plasma parameters considered in Fig. 7

The intensity measured by the detection system is the integral of the convolution of what is being emitted with the fraction that it is transmitted. The fourth plot of Fig.7 shows the profile of the integrand and gives not only the size of the emitting region but also the contribution of the different positions along the line of sight The differences observed between the three cases presented shows the dependence on the temperature and the density. An increase in the temperature makes the emission and absorption coefficients larger and broader, but also translates in a broader transmission, thus making the region contributing to the emission process broader. On the other hand, the linear dependence of the emission and absorption coefficients on the density does not change the shape of its profiles but only its high, thus decreasing the transmission (increasing the self-absorption) and reducing the size of the emitting region. Regarding the discussion about the relation between the frequency and the origin of the emission, please notice that for this frequency, f = 195 GHz, the naive resonant condition estimation gives R ≈ 297 cm while the maximum contribution to the emission ranges between 294 and 296 cm depending on the plasma parameters, and moreover its width ranges from 2 to 5 cm.

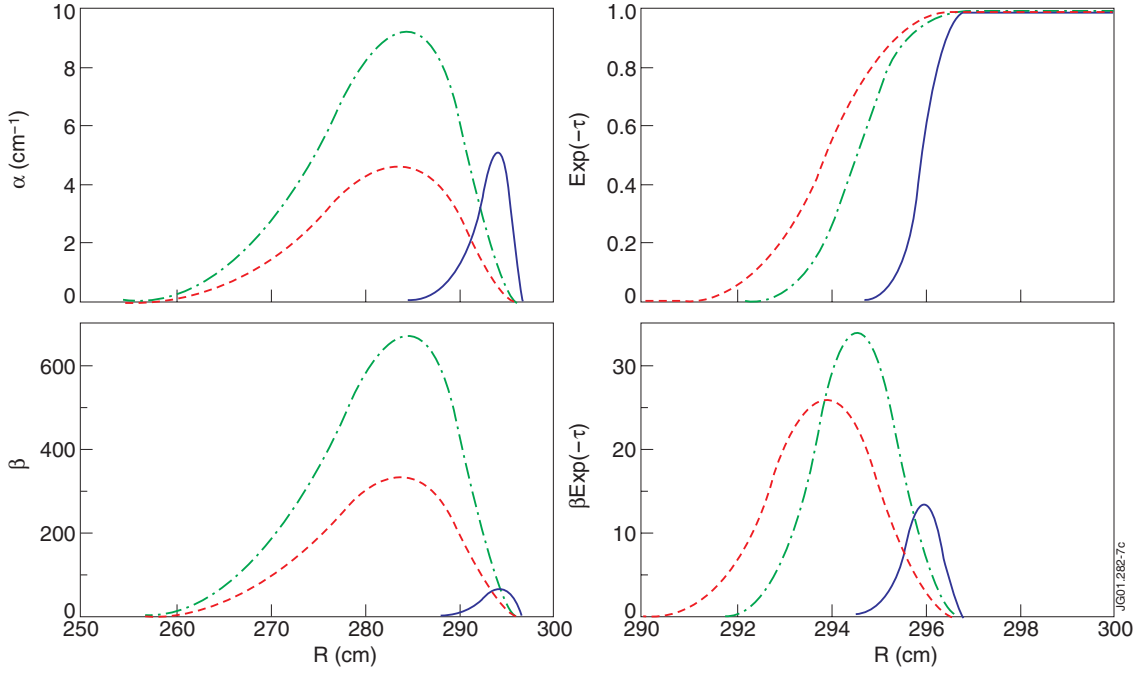

Figure.7: From top to bottom. Local absorption, emission, transmission and emitting coefficients versus the major radius for the parameters of Table 2: cases 1 shot #47413 (dotted), 2 (solid), and 3 (dashed).

In this work the spatial resolution of the EC emission is defined using (5) the integrand of the ECE, because this is the region contributing to the detected signal. Since the measured radiation intensity is an integral over a finite spatial region, the spatial localisation of the source of emission, for each frequency, can be estimated from the ray average as $\langle x(\mathbf{k}, \omega)\rangle = F(x(l), l_0, l_1)$, ($x = x$, y, z, or , R, φ, z) with the following definition for the auxiliary functional F:

$$F(x,a,b)= \frac{\int_a^b dl\, x(l)\beta(\mathbf{k},\omega,l)\exp\left(-\int_{l_0}^{l} dl\, \alpha(\mathbf{k},\omega,l)\right)}{\int_{l_0}^{l_1} dl\, (l)\beta(\mathbf{k},\omega,l)\exp\left(-\int_{l_0}^{l} dl\, \alpha(\mathbf{k},\omega,l)\right)} \tag{6}$$

and a measure of the spatial resolution of the ECE diagnostic by

$$\Delta^g x(\mathbf{k},\omega) = x(\mathbf{k},\omega,l^{max}) - x(\mathbf{k},\omega,l^{min}) \tag{7}$$

where l^{min} and l^{max}, satisfying

$$F(1,l_0,l^{min}) = (1 - g)/2$$
$$F(1,l^{max},l_1) = (1 - g)/2$$

are positions between which a certain fraction, g ($0 \le g \le 1$), of the total emission is produced. The operative definitions for the origin of the emission and the spatial resolution corresponds to the average value, the maximum for a symmetric curve, of the emitting profile, and the distance between the positions where a certain fraction of the total integral (emission) is originated. Both definitions are very reasonable in view of the Fig.7. In other branches of physics it is usual to define the width of similar profile functions with similar quantities, i.e.: the full width at half maximum (FWHM). What makes the calculations that are presented in this work somewhat different is that: i) the ECE detection system is only sensitive to the integral of the profile; ii) there is no simple relation between the plasma parameters and the profile shape; iii) the profiles is not necessarily symmetric. On the other hand the FWHM, or other definitions, are used for symmetric profiles where the dependence of the width on other physical parameters are known. This means that if we use Eq 7 to determine the spatial resolution with $g = 0.9$ (90% of the total emission) and our temperature is 10 keV between R^{min} and R^{max} only 9 keV are originated, and 1 keV is being emitted outside. Putting the emission in temperature units, see Eq.5, a pictorical view of the above mathematical expressions is presented in Fig.8.

The EC emission detected at a given frequency is originated in a finite plasma volume. Thus, even for the best possible conditions, only an average estimation of the electron temperature over the emitting region can be obtained.

1. The origin of the emission depends on the plasma parameters, and the condition $f = s f_c$ gives inaccurate results. A better estimation of the origin of the emission is given the average value defined in Eq 6.

2. The size of the emitting volume depends on the plasma parameters, and to determine its dimensions it is necessary to use a definition involving the integration of the profile, like in Eq 7.

Up to now no experimental constrains have been applied like:

(i) the finite antenna pattern of the detection system, which broadens the volume contributing to the emission and weights the importance of different regions.

(ii) the finite spectral width of the detection system, which averages the contribution of different frequencies, weighted with the shape of its apparatus function.

(iii) the shape of the plasma being diagnose, which sets some geometrical averages over the results.

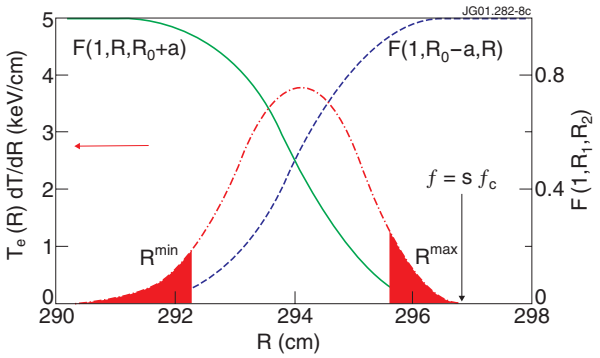

Figure.8: Integrand of Eq. 5 and the function F defined in Eq. 6, along with the values R^{min} and R^{max} for g = 0.9. The shadowed area corresponds to 10 % of the total emission.

(iv) the possible harmonic overlapping, which broadens the region contributing to the emission and makes the measurement almost useless to obtain local estimations.

In the next section these constrains will be taken into account in full ray tracing simulations.

4. RESULTS

Using the TRECE ray tracing code the spatial localisation and resolution will be presented, taking into account the real positions of the KK1 and KK3 diagnostics, its antenna pattern (using the Fraunhoffer diffraction pattern and considering a bunch of rays), for the shot #47413, with the real magnetic surfaces, calculated with the EFIT code, and the density and temperature profiles obtained with the main LIDAR Thomson scattering system. This shot was selected because of its relatively high electron temperature, and thus, the results that are presented correspond to the worst case.

In Fig.9, the average position <R>, see Eq. 6, and R^{min} and R^{max} corresponding to 90% of the signal (g = 0.9 in Eq.7), are plotted for the O and X-modes.

The general structure of both plots if Fig. 9 consist in sawthooth like curves representing the different harmonics, where the vertical parts correspond to the harmonic overlapping regions. In these frequency ranges it is still possible to define the average origin of the emission (solid curve) although the 90% of the signal comes from a spatial region covering most of the plasma (dotted lines). With the above simulation it is possible to identify the best operational conditions (detection mode and frequency range) of the ECE system to determine the local electron temperature. A closer look shows that in the first harmonic O-mode, between 75 and 140 GHz, and the second harmonic X-mode, and 150 and 210 GHz, the spatial resolution is fairly good (the three lines in Fig. 9 almost coincide). However, the radial coverage is quite different; from

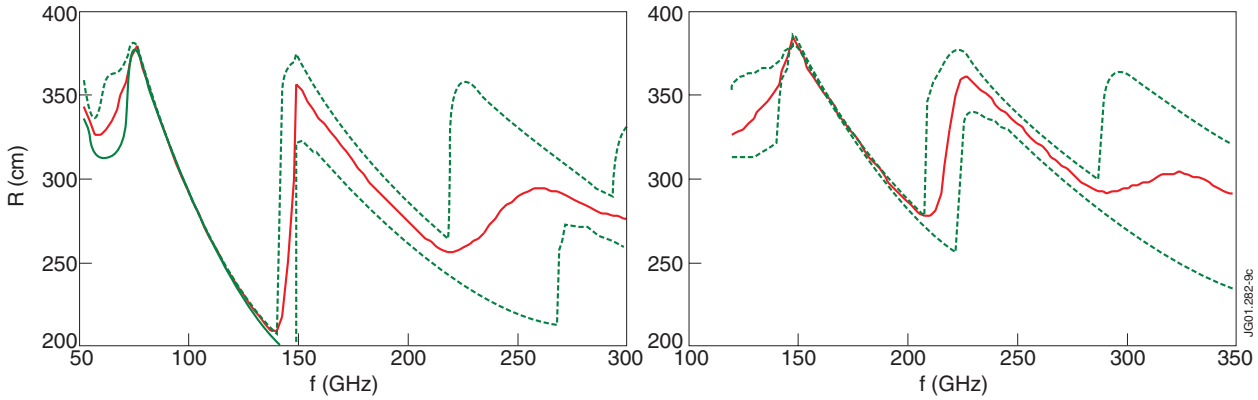

Figure.9: Average position <R> (solid), R^{min} and R^{max} (dotted) versus frequency for the O-mode (left) and X-mode (right) ECE of shot # 47413 simulated with the ray tracing code.

210 to 380 cm for the O-mode, and 280 to 380 cm for the X-mode. The X-mode can not access the inner side of the plasma because of the harmonic overlapping. The second, or third, harmonic contributions to the emission at the first, and second, harmonics enters from the low field side region ($R = R_0 + a$) at approximately 140, and 210 GHz, see Fig.10. The 1st harmonic resonance at 140 GHz is at $R \approx R_0 - a$ and thus the disturbance from the 2nd harmonic is minimum, but for 210 GHz the 2nd harmonic resonance is close to the plasma axis ($R \approx 298$ cm) thus for $f > 210$ GHz there is and overlapping between the 2nd and 3rd harmonics. The overlapping is even more severe for higher harmonics,because the radial variation of the s^{th} harmonic cyclotron frequency depends on the harmonic ($\mathrm{d}\, sf_c / \mathrm{d}R \approx - sf_c/R$).

In view of Fig.9 it is possible to explain another feature that was left open in the spectra shown if Fig.6, namely the appearance of the strong peaks at low frequencies for both the 1st harmonic O-mode and the 2nd harmonic Xmode. The origin of the emission moves outwards as the frequency decreases, see Fig.10, but bellow a certain minimum frequency, ≈ 75 GHz for the O-mode and 145 GHz for the X-mode, the origin of the emission begins to: move inward again thus giving higher temperatures, and broadens. Both effects can be explained remembering that: the energy of the resonant electrons depends on the difference between the local cyclotron frequency and the observation frequency, and the origin and localisation of the ECE is due to the self-absorption of the plasma, see Fig.7. There is some emission generated in the inside of the plasma, where the temperature is high, and thus where there are high energy electrons, that can not be reabsorbed by the electrons at the edge, because of the low and temperature. The overall effect is an inward shift of the emission origin and a broadening of the emitting region. For even lower frequencies the origin of the emission moves outward again and losses all the spatial resolution, because the required resonant energy is to high, even for the plasma bulk, and there is no self-absorption.

In computing the spatial location and resolution with the ray tracing code two different estimations can be used. Using the auxiliary function F it is possible to compute the averages for the major radius or for the flux surfaces. When only one ray in the equatorial plane of the plasma is considered both results are identical, since there is a one-to-one relation between major radius

and flux surfaces. However, when several rays are taken into account, or even for a single ray that does not cross the plasma axis, it is mandatory to use the flux surfaces estimate. The difference between the major radius and the equivalent major radius, deduced from the flux surfaces, for the JET tokamak, with its non-circular plasma cross section, is sketched in Fig.11.

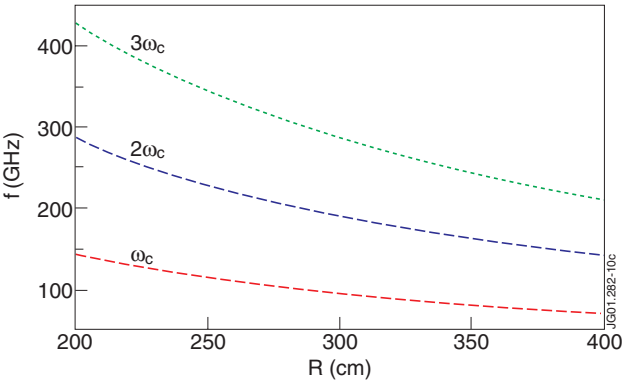

Figure.10: Radial dependence of the different cyclotron harmonics for the shot #47413.

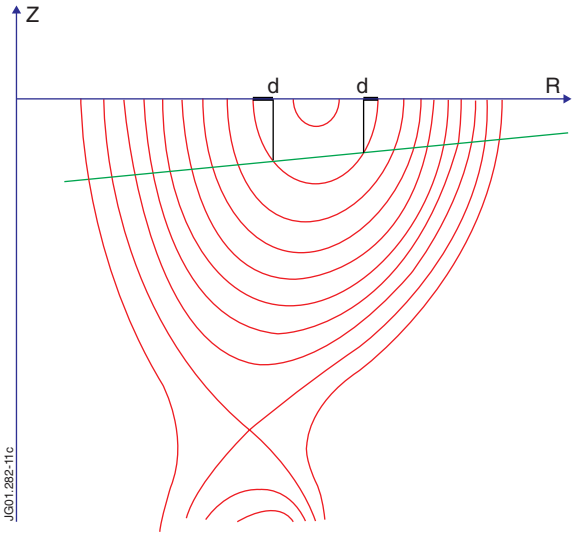

Figure.11: Sketch of the difference between the major radius and the equivalent radius corresponding to the flux surfaces

In Fig.12 the spatial resolution, simulated by the ray tracing code is presented for the Michelson interferometer (KK1) and the heterodyne radiometer (KK3) systems, using the origin of the emission as the abscissa.

The computed resolution, using the equivalent major radius, deduced from the flux surfaces, is always worst than the one obtained from the major radius except near the gap that appears close to the axis. On the KK3 system this gap is much larger than for KK1 because the rays do not cross the axis, see Fig. 5. The resolution of the X-mode is better than of the Omode because of its larger absorption for both systems.

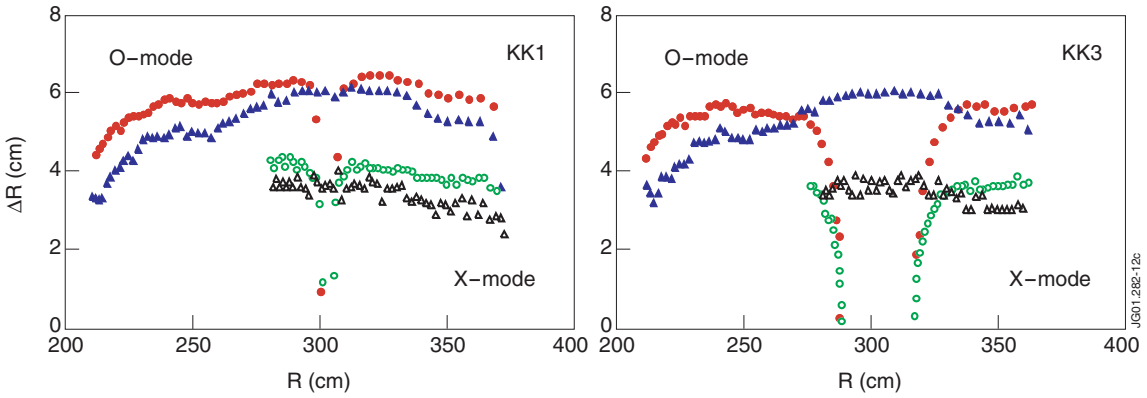

Figure.12: Spatial resolution, ΔR, obtained for the KK1 (left) and KK3 (right) systems for the geometrical major radius (triangles) and the equivalent major radius deduced form the flux surfaces (circles) and the O-mode (close symbols) and X-modes (open symbols), and the conditions of the shot #47413.

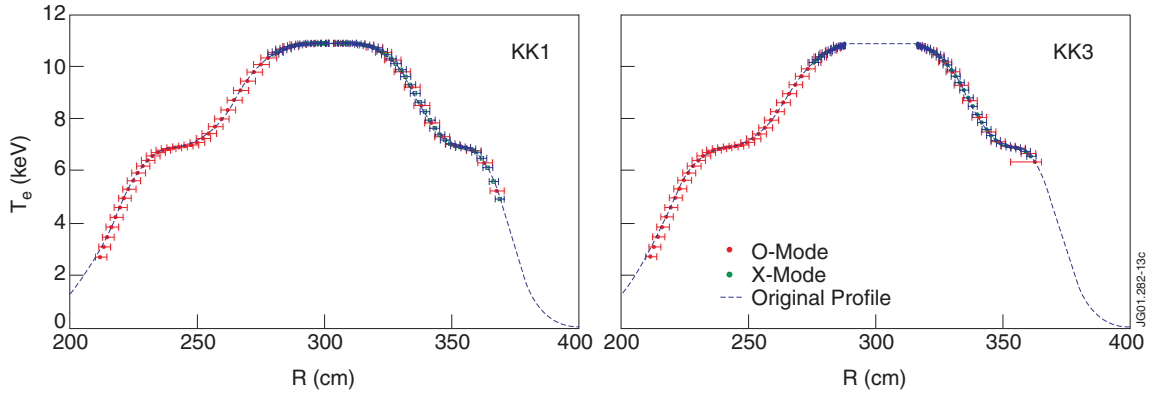

Figure.13: Simulated electron temperature profiles for KK1 and KK3 diagnostics with the original profile for the shot #47413. The error bars correspond to the spatial resolution of Fig.12.

The resulting simulated electron temperature profiles, obtained with the ray tracing code, are shown in Fig.13 for both the KK1 and KK3 diagnostics for the O and X-modes.

The radial position has been computed using the equivalent major radius, deduced from the flux surface and the magnetic field, and the error bars indicate the region where 90% (g = 0.9) of the emission is generated. As a general result we see that the O-mode emission covers most of the plasma profile, whereas the X-mode coverage is limited by the harmonic overlapping. The noticeable gap in KK3 results is due to the fact that its line of sight does not cross the plasma axis, see Figs.5 and 12. A better view of the effect of considering the cold resonant position and the radial position directly from the major radius, instead of the equivalent major radius, is presented in Fig.14 for three different radial ranges and the Xmode emission simulated for KK3. From physical and geometrical reasons it has been established that for expressing the EC emission

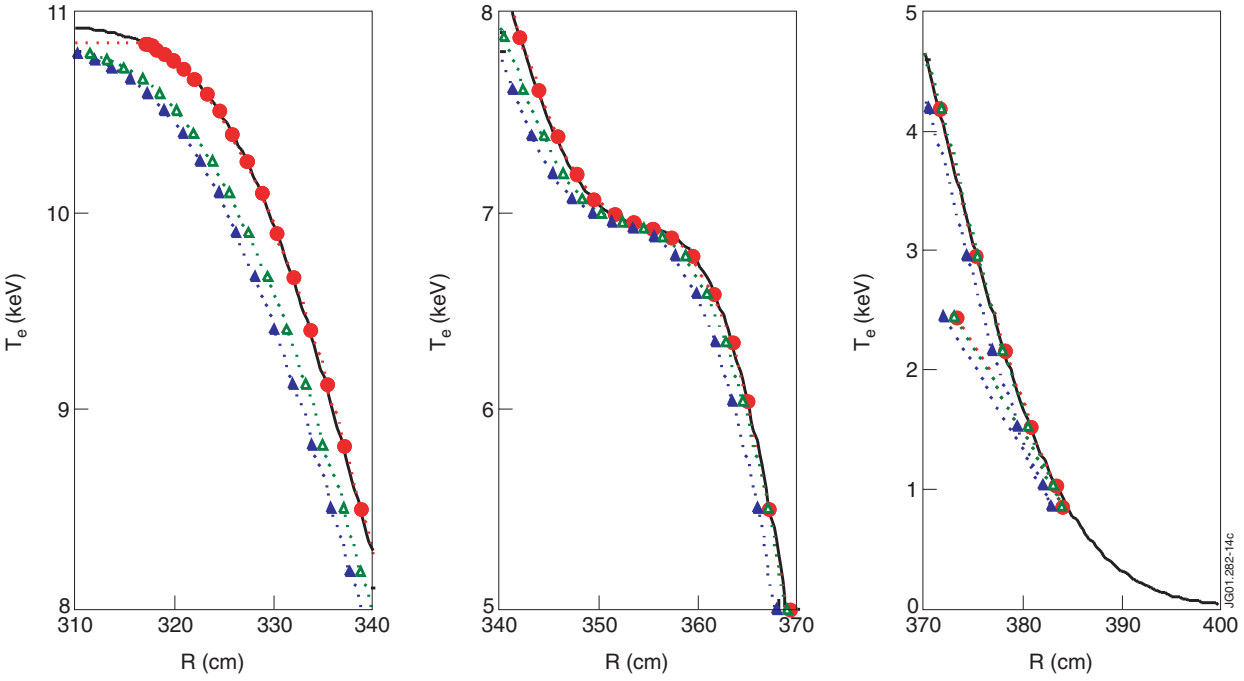

Figure.14: Original (solid) and simulated electron temperature profiles for KK3, for the equivalent major radius (full circles), major radius(full triangles) and major radius for the cold resonance position (open triangles) corresponding to the conditions of Fig. 13 and the X-mode emission.

spectra as a temperature profile it is necessary to use the average value of the emission in flux surfaces and then make the translation to major radius. However, from Fig.14 it seems that in the outer part of the plasma using the wrong cold resonance position directly in major radius is a good approximation. This is due to a cancellation between using two bad approximations; please notice that this cancellation does not occur in the plasma core. Actually, the distance between the cold resonance position and the mean value of the emission, Eq.6, is shown in Fig.15.

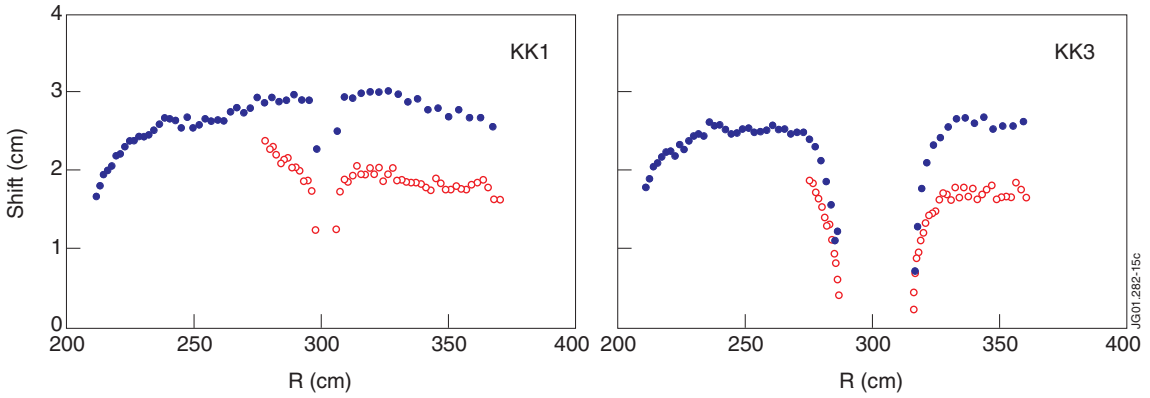

Figure.15: Distance between the cold resonance position and the average origin of the emission obtained for the KK1 (left) and KK3 (right) systems for the equivalent major radius deduced form the flux surfaces and the O-mode (close symbols) and X-modes (open symbols), and the conditions of the shot #47413.

Please notice that through these simulations a monochromatic detection frequency is assumed, in contrast, the heterodyne radiometer detection system (KK3), has a set of filters with a bandwidth of 250 MHz. Assuming a magnetic field depending of $1/R$ the broadening due to these filters can be estimated as: $\Delta R \approx R/s f_c \Delta f$, see Fig.16 (left). The contribution of these 250 MHz filters, with a step like shape, to the broadening depends not only on the harmonic but also on the major radius, because of the magnetic field gradient. The frequency distance between consecutive channels in the system, 500 MHz, has been optimised to fully cover the spectra. Using the same argument as with the bandwidth the equivalent distance, along the major radius, between consecutive channels is plotted in Fig.16 (right).

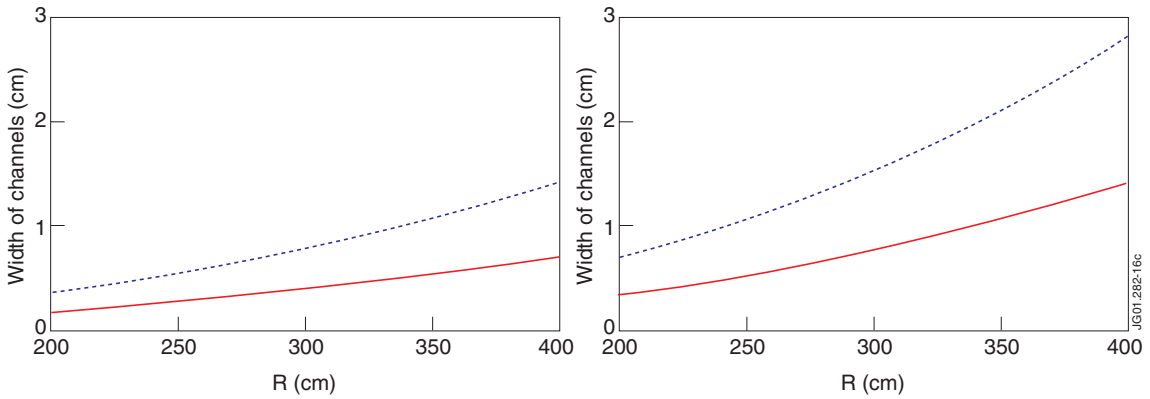

Figure.16: For the heterodyne radiometer (KK3), spatial width (on the left) due to the 250 MHz IF bandwidth of the filters, and distance between consecutive channels, separated 500 MHz, versus the radial position.

It is interesting to note that although: the origin of the emission is shifted by ≈ 2 and 3 cm, for the X- and O-modes, with respect to the cold resonance position, see Fig.14; the region contributing to the EC emission is ≈ 4 and 6 cm broad, see Fig.12 (actually it is a little bit larger if the bandwidth of the filters is included) nevertheless the channels are separated, at best, but only 0.8 - 1.5 cm (X-mode) and 0.8 - 3 cm (O-mode).

Another interesting point concerns the use of the ECE to accurately determine the edge electron temperature in high confinement regimes. To clarify this point ray tracing simulations, made using the above methodology, have been performed for the shot #50486, see Fig.17.

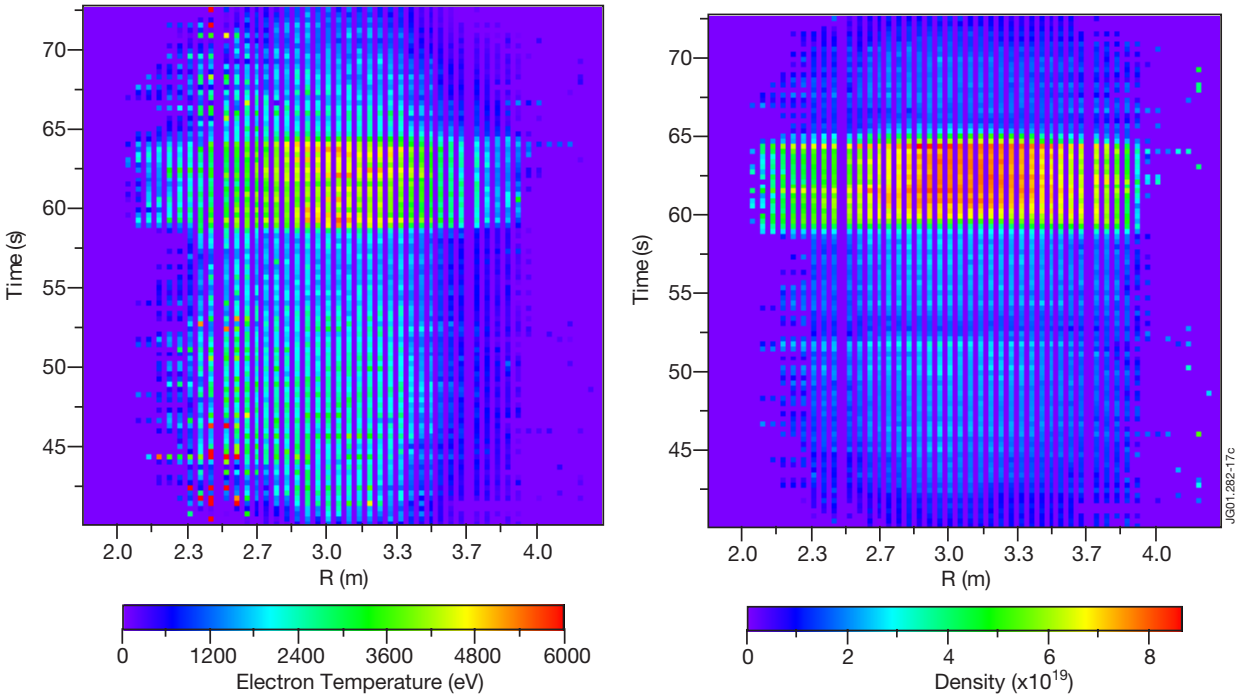

Figure.17: Spatial and temporal evolution of the electron temperature, on the right, and density, obtained with the LIDAR system for the shot # 50486.

The density and temperature profiles, corresponding to t = 60.625 s, have been fitted in normalised magnetic flux with the help of the EFIT code, Fig.18, and the ECE spectra obtained from the ray tracing simulation is plotted in Fig.19. The origin of the emission, obtained through eq. 6 and 7 for the spectra of Fig.19 is presented in Fig 20.

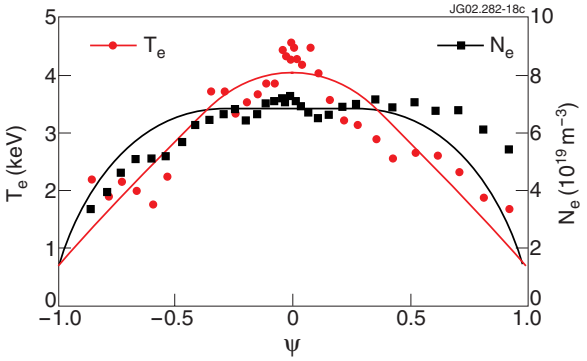

Figure.18: Electron temperature and density profiles for the shot # 50486 at t=60.625 s.

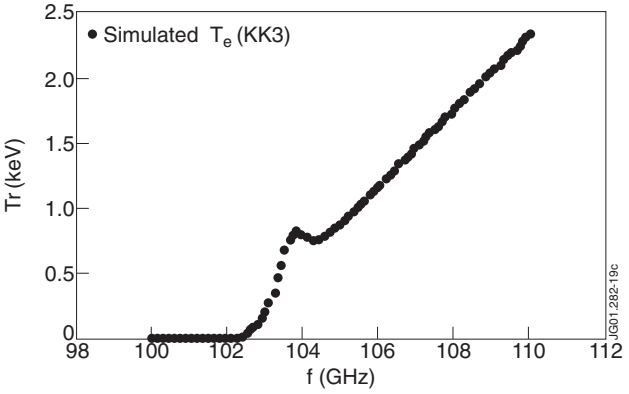

Figure.19: Electron cyclotron emission spectra obtained by ray tracing simulation for the profiles of Fig.18.

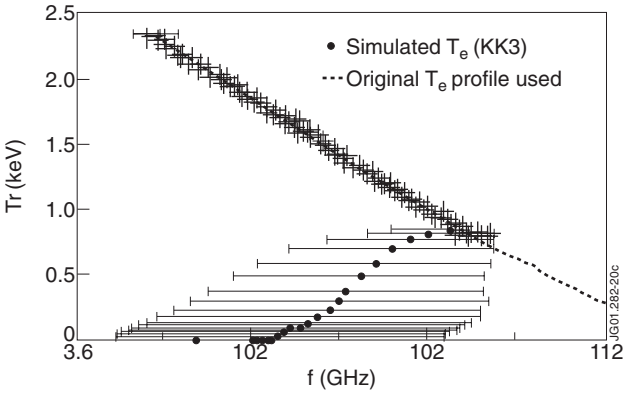

Figure.20: Electron temperature profile at the edge obtained from the ray tracing simulation, taking into account the origin of the emission. The original profile used in the simulation is also included for consistency. The error bars indicate the region where 90% of the emission is originated

From Fig.20 it is clear that the bump that appears in the emission spectra, and that can be wrongly interpreted as a bump in the edge electron temperature, is due an inward shift of the origin of the emission, due to a decrease in the self-absorption because of the small density and temperatures at the edge. Moreover, there is also a broadening in the region contributing to the emission and a degradation in the spatial resolution of the diagnostic (indicated with the error bars in Fig.20).

5. CONCLUSIONS

The spatial resolution of the electron cyclotron emission phenomena has been discussed including the underlying physical process and the experimental constrains (i.e.; antenna pattern, filters bandwidth, …). A working definition based on the spatial structure of the emission profile has been presented allowing estimating the origin of the EC emission and its size. The method has been applied to a typical JET pulse (#47413) using a three dimensional ray tracing code, where all the relevant effects have been included.

The estimated spatial resolution of the actual EC systems in use at JET, for the pulse considered, is found to be of approximately 6 cm for the 1st harmonic O-mode and around 4 cm for the 2nd harmonic X-mode. These values can be considered as lower bounds since they do not include the finite bandwidth of the experimental set-up (0.2 - 1 cm for the X-mode and 0.5 - 1.5 cm for the O-mode), and only a simple diffraction model for the antenna pattern has been used.

The resolution decreases for increasing temperature and decreasing density, for fixed magnetic field gradient and–*N*||. In this way the estimations for the spatial resolution can be extended from the pulse considered to other plasma parameters, since the actual profile used contains quite different densities and temperatures.

The capabilities of the ECE to accurately measure the edge electron temperature has also been addressed with a ray tracing simulation taking into account the origin and width of the

emitting layer for a given frequency. It is shown that bump-like effects appearing in the ECE spectra can be attributed to an inward shift of the origin of the emission rather than to a real structure in the electron temperature.

ACKNOWLEDGEMENTS

This work has been performed under the European Fusion Development Agreement. The author would like to thank all the members of the *electron* group: M. Alonso, M. Beurskens, G. Conway, J.M. Chareau, J. Fessey, C. Gowers, G. Granucci, L. Meneses, C. Nicholson, R. Prentice, J.L. Segui, O. Tudisco and M. Zerbini.

REFERENCES

[1]. M. Bornatici, R. Cano, O. De Barbieri and F. Engelmann, *Nuclear Fusion* **23** 1153 (1983)

[2]. G. Bekefi, *Radiation Processes in Plasmas*, (John Willey & Sons, NewYork 1966)

[3]. D.P. O'Brien, L.L. Lao, E.R. Solano, M. Garriba, T.S. Taylor, G. Cordey and J.J. Ellis*, Nuclear Fusion* **32** 1351 (1992). W. Zwingmann, D.P. O´Brien and D. Bartlett*,* Proc. 7th European Fusion Theory Conference, Jülich (1997). V. Drozdov, *Personal communication* (2000)

[4]. C. Gowers and M. Beurskens , *Personal communication* (2000)

[5]. V. Tribaldos and B. Ph. Van Milligen, *Nuclear Fusion* **36** 283 (1996)